Magnetism in Ar-implanted ZnO

2007 J. Phys.: Condens. Matter 19 476207

(http://iopscience.iop.org/0953-8984/19/47/476207)

J. Phys.: Condens. Matter **20** (2008) 429801 (1pp) doi:10.1088/0953-8984/20/42/429801

Corrigendum

Magnetism in Ar-implanted ZnO

R P Borges, R C da Silva, S Magalhães, M M Cruz, M Godinho

J. Phys.: Condens. Matter **19** 476207

The authors have detected an error in the graph of figure 1 in the above paper. Both vertical scales should be multiplied by a factor of 10. All values related to the graph mentioned in the text are correct. However, a reader analysing the present graph will find values that are 10 times smaller than they should be.

IOP PUBLISHING JOURNAL OF PHYSICS: CONDENSED MATTER

J. Phys.: Condens. Matter **19** (2007) 476207 (12pp) doi:10.1088/0953-8984/19/47/476207

Magnetism in Ar-implanted ZnO

R P Borges[1], R C da Silva[2,3], S Magalhães[4], M M Cruz[1,5] and M Godinho[1,5]

[1] Centro de Física da Matéria Condensada-Universidade de Lisboa, Campo Grande, Ed. C8, 1749-016 Lisboa, Portugal
[2] Laboratório de Feixe de Iões, Dep. Física, Instituto Tecnológico e Nuclear, Estrada Nacional 10, 2686-953 Sacavém, Portugal
[3] Centro de Fisica Nuclear da Universidade de Lisboa, Av. Prof. Gama Pinto 2, 1649-003 Lisboa, Portugal
[4] Instituto Tecnológico e Nuclear, Estrada Nacional 10, 2686-953 Sacavém, Portugal
[5] Dep. de Física, Faculdade de Ciências, Universidade de Lisboa, Campo Grande, Ed. C8, 1749-016 Lisboa, Portugal

E-mail: rpborges@fc.ul.pt

Received 15 June 2007, in final form 27 September 2007
Published 31 October 2007
Online at stacks.iop.org/JPhysCM/19/476207

Abstract

ZnO single crystals were implanted with Ar ions with an energy of 100 keV and different fluences. Ferromagnetic behaviour is observed at room temperature after implantation. This behaviour is suppressed after consecutive annealings at 400 and 500 °C. Although trace transition metal impurities have been identified in the virgin samples, it is shown that they cannot account for the observed magnetic behaviour that is assigned to the presence of implantation-induced lattice defects.

1. Introduction

Spin electronics uses the long spin coherence length of electrons to create devices that carry information using spin as well as charge. Much attention has been devoted to materials that can carry a highly spin polarized current such as the colossal magnetoresistance perovskites. However, ferromagnetic–semiconductor junctions have shown poor results regarding spin injection into the semiconductor. An alternative has been sought in diluted magnetic semiconductors (DMSs), in which ferromagnetism arises from the doping of a non-magnetic semiconductor with a transition metal element, as predicted for the case of Mn-doped ZnO [1].

The mechanism leading to ferromagnetism in these materials is not yet clear, and there is a wide spread of results published by different groups [2]. One of the issues is the formation of secondary phases that could be responsible for many of the reports of ferromagnetism in magnetic semiconductors [3]. However, the presence of ferromagnetic ordering in a variety of systems that do not include magnetic elements such as HfO_2 [4] and $Ca_{9.995}La_{0.005}B_6$ [5], together with band structure calculations showing that in CaO [6] and HfO_2 [7] a cation

vacancy may be associated with a magnetic moment, have led Coey to propose a model of ferromagnetism based on lattice defects [8]. The defects are both responsible for the formation of a magnetic moment at the molecular orbitals surrounding the vacancy and for the formation of an impurity band that can mediate a long range ferromagnetic ordering of the moments. In ZnO doped with different transition metal ions, defects have also been proposed as one of the contributing factors for ferromagnetic interactions. Ferromagnetism has been observed in doped ZnO systems with structural defects, such as thin films and implanted crystals, but it is not proved to exist in well crystallized diluted systems [9]. A study where Co-doped ZnO is subjected to alternate annealings in Zn vapour and oxygen shows the appearance and disappearance of the magnetism [10]. In the case of another doped system, magnetism in colloidal Ni-doped ZnO can be activated by interparticle grain-boundary defects [11]. Room temperature ferromagnetism has been observed in non-doped ZnO thin films grown by pulsed laser deposition and is attributed to Zn defects [12]. Further evidence of magnetic ordering in non-doped oxides has been provided by studies of CeO_2, Al_2O_3, ZnO, In_2O_3 and SnO_2 nanoparticles [13]. The authors find that these nanoparticles are ferromagnetic and attribute the ferromagnetism to the exchange interactions between unpaired spins resulting from oxygen vacancies at the nanoparticle surface. When the particles are annealed at high temperatures, their volume increases and the ferromagnetism disappears. Ferromagnetic behaviour was also reported in non-doped ZnO nanoparticles after capping with different organic molecules [14]. The magnetic behaviour associated with the presence of defects is supported by a recent report on Si wafers that display ferromagnetism at room temperature after being implanted with Si and Ar ions or irradiated with neutrons [15]. Given the absence of transition metal ions, the authors attribute the ferromagnetic signal to the dangling bonds caused by irradiation.

In this work the implantation of Ar ions into ZnO single crystals was investigated in order to study their contribution to the magnetic properties of the material. We expect this implantation to induce a large concentration of lattice defects. Since Ar ions do not carry a magnetic moment, any magnetic behaviour that may develop cannot be assigned to the implanted ions but has to be considered a consequence of implantation generated defects.

2. Experimental details

Commercial ZnO single crystal substrates ($5 \times 5 \times 0.5$ mm^3) with (001) orientation from the same batch were used. Some of these crystals were implanted with Ar ions with implantation energy of 100 keV and fluences of 1×10^{16}, 1×10^{17} and 2×10^{17} Ar cm^{-2}. The masses of the crystals are between 64 and 67 mg in all cases.

X-ray diffraction (XRD) patterns in the θ–2θ geometry were obtained using Cu Kα_1 radiation. The beam divergence was 0.001° and the diffracted beam was captured using a PSD detector. To access modifications in the implanted layer, XRD reciprocal space analysis was performed.

In order to check for the presence and concentration of impurities—namely magnetic impurities—the ZnO crystals were analysed by particle induced x-ray emission (PIXE) spectrometry, both before and after implantation. PIXE analysis was performed with protons of energy 1.5 MeV, with an incidence angle of 22.5° relative to the surface normal. A Si(Li) detector with 145 eV energy resolution was used to record the x-ray spectra at an angle of 135° to the incident beam direction.

Magnetic characterization was carried out using a Quantum Design SQUID magnetometer. $M(H)$ curves were obtained in magnetic fields up to 1.0 T, sufficient to saturate the magnetization. Measurements of magnetization were made as a function of temperature, $M(T)$, between 10 and 300 K. Magnetization curves at 0.01, 0.05 and 0.1 T were obtained

after cooling the sample in zero magnetic field (zero field cooled—ZFC) and after cooling the sample under the measuring field (field cooled—FC).

3. Results and discussion

Simulations of the implantation profiles using the Monte Carlo code SRIM were carried out for the implantation of 100 keV Ar ions into ZnO. The simulations predict nearly Gaussian Ar distributions, only slightly skewed and flattened, centred at a depth of 63 nm and with a FWHM of 64 nm. The corresponding implantation generated damage—vacancies and interstitials—is predicted to extend from the surface to 100 nm depth, peaking around 40 nm, with ∼40% more Zn vacancies and interstitials than O defects of the same type. The results of these simulations are displayed in figure 1.

ZnO crystallizes with a wurtzite type structure with $P6_3mc$ group symmetry and lattice parameters $a = 0.324\,982$ nm and $c = 0.520\,661$ nm. X-ray diffraction patterns were taken in the θ–2θ geometry for both virgin and implanted samples. The results show only the (002) and (004) peaks as expected for well oriented crystals, with no evidence of secondary phase formation in the implanted samples. For these samples, x-ray reciprocal space maps (figure 2) exhibit an expansion of the truncation rod for lower q_z, indicating an increase of the c parameter at the surface layer of the crystal. This expansion is approximately 0.1% independently of implantation fluence (see table 1). The lattice parameter a remains unchanged for all samples.

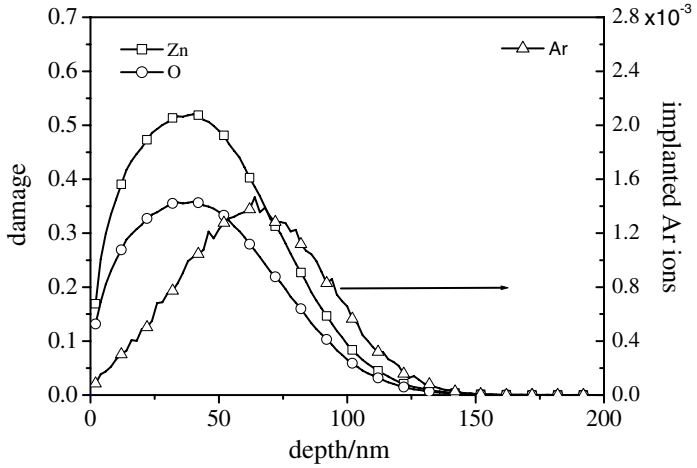

Figure 1. Implanted Ar and damage distribution profiles in ZnO simulated using the SRIM code. The Ar ion concentration is predicted to peak at a depth of 63 nm and have a full width at half maximum (FWHM) of 64 nm. Most of the implantation generated defects distribute from the surface to 100 nm. The total damage, vacancies and interstitials of both O and Zn, amounts to ∼600/Ar ion. Units are number/ion/nm.

Table 1. Lattice parameters a and c of virgin and implanted crystals obtained from the (004) and (105) reflections. All values are expressed in nanometres.

	Virgin crystal	1×10^{16} Ar cm^{-2}	1×10^{17} Ar cm^{-2}	2×10^{17} Ar cm^{-2}
(004) c	0.520 24	0.521 04	0.521 04	0.521 09
(105) a/c	0.325 04/0.520 23	0.325 04/0.521 06	0.325 04/0.521 06	0.325 01/0.521 08

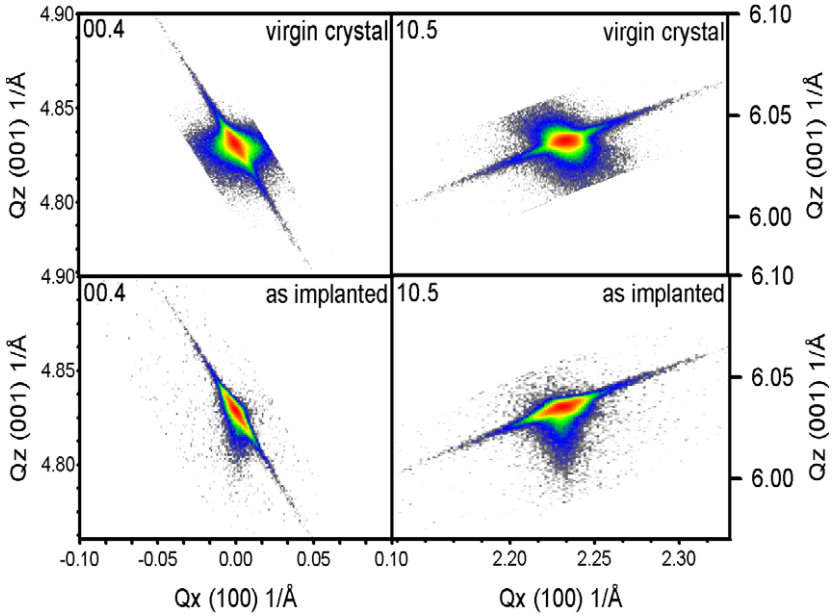

Figure 2. X-ray reciprocal space maps of ZnO crystals. The maps for the (004) diffraction peak are shown on the left and the ones for the (105) diffraction peak are shown on the right. The top maps correspond to the virgin crystal and the bottom maps correspond to the crystal implanted with a fluence of 2×10^{17} Ar cm^{-2}.

(This figure is in colour only in the electronic version)

Table 2. Impurity concentration of virgin crystal and crystal implanted with 1×10^{17} Ar cm^{-2}.

	Ti (ppm)	Cr (ppm)	Mn (ppm)	Fe (ppm)	Ni (ppm)
Virgin substrate	<10	<20	<35	160	210
1×10^{17} Ar cm^{-2}	27	35	45	190	160

PIXE was used in order to identify eventual impurities present in the crystals. The spectra shown in figure 3 are for a virgin crystal and for a crystal implanted with 1×10^{17} Ar cm^{-2}. In both cases peaks related to Cr, Mn, Fe, Ni and Cu can be observed. For the implanted crystal, two additional peaks are visible at energies of 2.96 and 3.19 keV, which are associated respectively with the K_α and K_β emissions from Ar ions. The concentration of impurities was determined by fitting the PIXE spectra with the analytical package GUPIX [16]. The results are presented in table 2 and show that Ni and Fe are the main impurities. The similarity between the spectra of implanted and non-implanted crystals excludes the possibility of Fe or Ni contamination during the implantation procedure. The levels of impurity concentration measured (<0.04 at.%) are much lower than any value reported for doped samples.

For all samples the magnetization results exhibit a diamagnetic signal as a major contribution attributed to the non-implanted ZnO. The DC susceptibility of virgin ZnO crystals was determined at different temperatures and verified to agree within 3% with the reported value for the diamagnetic susceptibility of ZnO, $\chi_{ZnO} = -3.34 \times 10^{-7}$ emu g^{-1} Oe^{-1} [17]. In order to isolate the magnetic contribution of the implanted region, the diamagnetic signal of the non-implanted part was subtracted from the raw measurements. Since the implanted

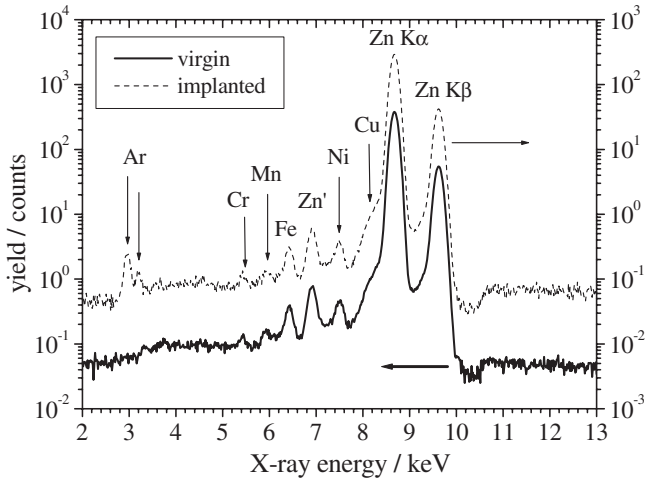

Figure 3. Particle induced x-ray emission (PIXE) spectra of ZnO implanted with 1×10^{17} Ar cm^{-2} (dashed line) and a virgin crystal (solid line).

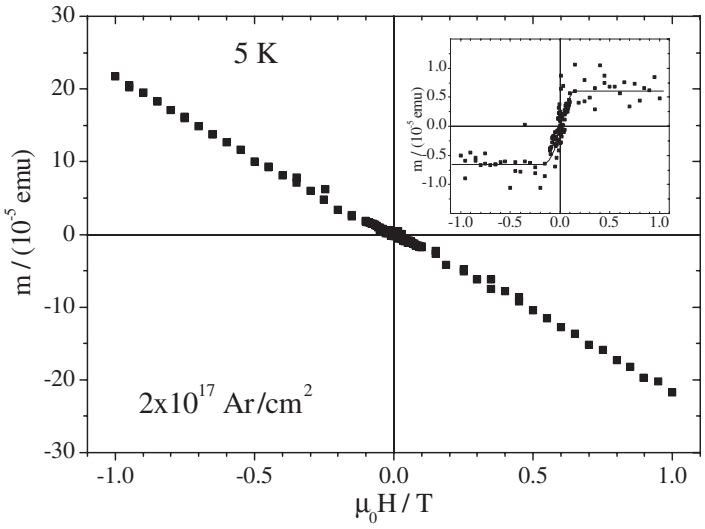

Figure 4. $M(H)$ data obtained at 5 K for the sample implanted with 2×10^{17} Ar cm^{-2} before removal of the diamagnetic component of ZnO (main) and after subtraction of this component (inset).

region is only a very small fraction of the crystal volume (∼0.02%), this was accomplished using the reported susceptibility value and the mass of each crystal. Figure 4 shows the raw data obtained for the sample implanted with 2×10^{17} Ar cm^{-2} compared to the curve obtained upon subtraction of the diamagnetic component of ZnO. All the experimental magnetic results presented here (with the exception of figure 4) already include this correction.

Field cooled magnetization for the implanted crystals is shown in figure 5. The data for the sample implanted with the lower fluence, 1×10^{16} Ar cm^{-2}, show, after correction for the ZnO diamagnetic moment, a large dispersion around a small positive value and almost no variation with the value of the applied field. For the two samples implanted with higher

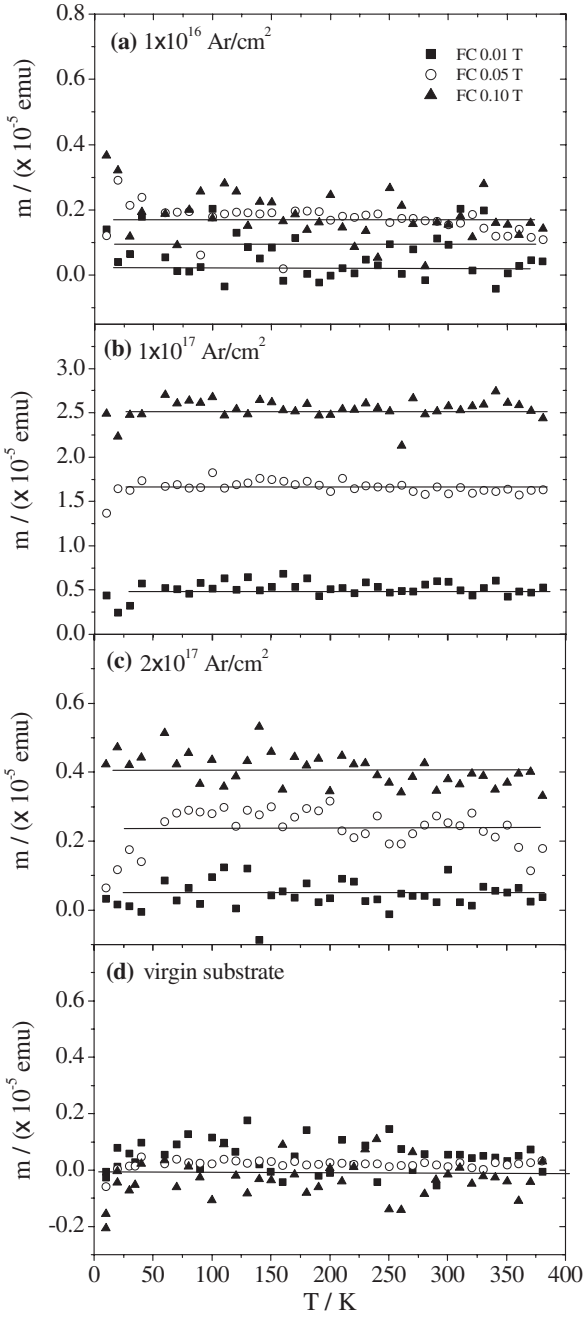

Figure 5. Field cooled magnetization of the implanted samples and a virgin crystal. In all cases the diamagnetic moment of ZnO has been subtracted. Lines are guides to the eye.

fluences it is clear that a positive and approximately constant magnetic signal, which increases with the applied magnetic field, is present over the whole range of temperatures. The associated magnetic moment is higher for the sample implanted with a fluence of 1×10^{17} Ar cm^{-2}. It

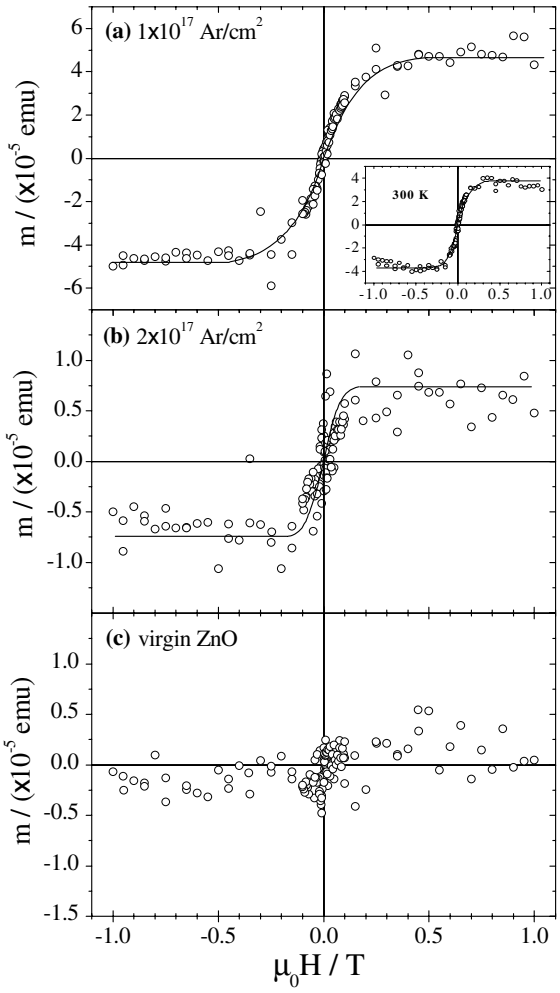

Figure 6. Magnetization measured at 5 K for the samples implanted with (a) 1×10^{17} Ar cm^{-2} and (b) 2×10^{17} Ar cm^{-2} and (c) for a virgin substrate. The inset of (a) shows the magnetization curve measured at 300 K. The large scattering of the data points is an artefact due to the simple subtractive method used for eliminating the diamagnetic contribution of the unimplanted bulk ZnO, as explained in the text. Lines in (a) and (b) are a guide to the eye.

is also clear from the curves for the higher implantation fluences that the positive magnetic moment remains approximately constant up to temperatures above room temperature. In the case of the virgin crystal (figure 5(d)), the removal of the ZnO diamagnetic contribution brings the magnetization to zero, indicating that the Fe and Ni impurities detected by PIXE do not give a magnetic contribution to the properties of the unimplanted ZnO. The large relative scattering observed in the presented experimental values results from the fact that they are obtained by subtraction of the ZnO diamagnetic contribution of each crystal (the raw signal is generally one order of magnitude larger).

Measurements of the magnetic moment as a function of applied field were taken at 5 and 300 K and are shown in figure 6. The data for the sample implanted with the lower fluence are not shown since they are very scattered with no clear trend. The largest and most pronounced

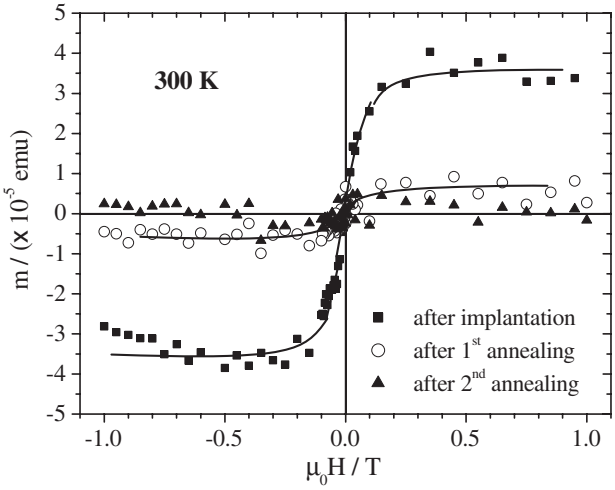

Figure 7. Room temperature magnetization of the sample implanted with 1×10^{17} Ar cm^{-2}: after implantation (solid squares), after annealing in air at 400 °C for 6 h (open circles) and after a second annealing in air at 500 °C for 6 h (stars).

$M(H)$ response is obtained for the sample implanted with 1×10^{17} Ar cm^{-2}. For the highest implantation fluence (2×10^{17} Ar cm^{-2}) a similar behaviour is observed but with a significantly smaller saturation value for the magnetic moment. The same pattern is reproduced at 300 K for both samples. In the case of the virgin sample, at 5 K, the magnetic moment falls to values below 1×10^{-6} emu at 1 T, indicating that no magnetic order or significant paramagnetic contributions are present.

The implanted samples were annealed in air at 400 °C for 6 h and further annealed in air at 500 °C for another 6 h. The resulting magnetization curves, presented in figure 7 for the case of the 1×10^{17} Ar cm^{-2} implanted sample, show the decrease of the magnetic moment after the first annealing and the vanishing of the magnetic ordering after the second one.

The data presented above show two important features. The first is the onset of a strong magnetic moment after implantation with non-magnetic ions. The second is the suppression of this moment by thermal annealing. Two mechanisms can be put forward to explain the onset of the magnetic moment. The first is the formation of magnetic aggregates or secondary phases from the impurities in the samples, and the second one is the influence of defects that can be assigned to a magnetic moment.

The possible role of the transition metal impurities requires some previous discussion. The expected paramagnetic contribution of the most relevant native impurities, Fe and Ni, was calculated assuming substitutional ions, Fe^{2+} and Ni^{2+}. Considering these ions in the substitutional tetrahedral positions, Fe^{2+} has a ^5E ground state ($S = 2$) and Ni^{2+} has a $^3T_1$ ground state ($S = 1$). The d bands are split by the crystalline field and the doubly degenerate e_g orbitals have lower energy. In such a case the spin-only magnetic moments are 4.90 μ_B for Fe^{2+} and 2.83 μ_B for Ni^{2+}. The corresponding magnetic moment value for the paramagnetic contribution of Fe and Ni impurities assumed to be homogeneously distributed in the whole volume of the sample is as high as 2.2×10^{-3} emu at 5 K and 1 T. The experimental results for a virgin crystal (figures 5 and 6) clearly exclude this possibility, indicating that the ions are magnetically inert. This conclusion is corroborated by results on Fe and Cu co-doped zinc oxide, indicating that the majority of the Fe ions are magnetically inert [18]. A possible

explanation could be the strong hybridization between the d orbitals of the transition metal ion and the p orbitals of the surrounding oxygen ions, with the consequent sharing of the 3d electrons and a significant decrease of the magnetic moment as observed in co-doped ZnO nanorods [19]. Several authors have also reported the absence of ferromagnetic order in single phase bulk ZnO doped with transition metal ions, observing only a paramagnetic signal for a high dopant concentration [20–23].

One should now consider the problem of aggregation or secondary phases. Although the impurities are magnetically inert before implantation, one can claim that the implantation might modify the magnetic behaviour of the diluted impurities by promoting aggregation. Since the lattice damage extends to a depth of the order of 100 nm, a region that includes most of the implanted Ar ions and represents 0.02% of the total volume of the crystals, only Ni and Fe ions inside this volume must contribute to the formation of such precipitates. The corresponding total magnetic moment calculated considering the added contribution of Ni and Fe ferromagnetic aggregates is 1×10^{-6} emu, a value that represents one-fifth of the magnetic moment measured for the sample implanted with 2×10^{17} Ar cm^{-2} and 50 times smaller than the moment obtained for the sample implanted with a fluence of 1×10^{17} Ar cm^{-2}. The calculated magnetic moment for aggregates of ferrimagnetic oxides like Fe_3O_4 is also much lower than the measured values. Ferromagnetic aggregates would have sizes above a critical dimension (10–15 nm), in which case they should be visible in XRD patterns [3]. The same considerations regarding size would apply if the aggregates were to be intrinsic to the crystals and their magnetic state was being altered by the Ar implantation. No corresponding diffraction peaks were detected. Given the very low impurity concentrations, the formation of aggregates with nanosize dimensions could explain the absence of x-ray diffraction peaks. However, such nanosized particles would have superparamagnetic behaviour. There is no evidence of such behaviour in the magnetization temperature dependence of any of the virgin or implanted crystals (figure 5). Reports on ion-implanted ZnO with higher concentrations of transition metals such as Co [3], Fe [24] and Ni [25] indicate that thermal annealings induce the growth of aggregates. This indication does not fit the observed suppression of the moment with thermal annealing. Considering these arguments, the data presented do not support an explanation of the observed ferromagnetic behaviour by magnetic nanoparticle formation, indicating that its origin must lie elsewhere.

As previously mentioned, the role of defects in oxides has been discussed recently. A general model for explaining ferromagnetism in semiconducting oxides based on the contribution of lattice defects has been proposed [8]. If a large enough number of such defects exists then an impurity band can be formed. If this band has a large density of states, such that the Stoner criterion $D(E_F)I > 1$ is satisfied, then a spontaneous spin splitting of the band can occur. Alternatively, defect states can have associated magnetic moment, such as those identified in CaO [6] and HfO_2 [7]. These states could create an impurity band that would mediate the long range ferromagnetic ordering. Both mechanisms might be present in our Ar-implanted ZnO, since the high fluences used are clearly associated with a high defect density that can lead to the formation of a defect band. Note that in our samples modifications occur in a region extending to about 100 nm in depth, indicating that the behaviour is not a surface effect as in the case of the reported results for nanoparticles. However, the similarity between the $M(T)$ curves presented here and those shown in [14], i.e. the thermally independent behaviour of magnetization, are an indication that our results belong to the same family of phenomena. Furthermore, a bulk effect associated with lattice defects with the same thermal independence of magnetization has been observed in proton-irradiated graphite [26].

To characterize the evolution of the damaged region specular x-ray reflection measurements were performed; figure 8 shows the specular x-ray reflection path of the

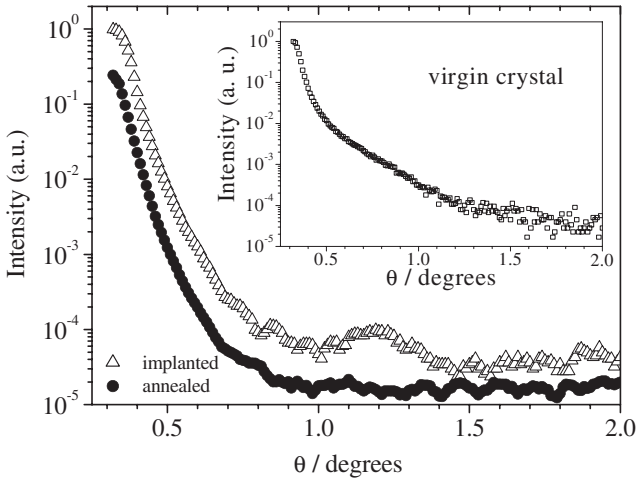

Figure 8. Specular x-ray reflection path of the incoming beam for a virgin ZnO crystal (inset), and for the same crystal after implantation with Ar and after two annealings in air at 400 and 500 °C.

incoming beam for the situations analysed in this work: virgin crystal, implanted with 100 keV Ar ions, and after two consecutive annealings in air at 400 and 500 °C. The curves show the reflectivity of the first 100 nm of the crystal surface, where most Ar ions and defects are located. The virgin crystal shows a typical bulk crystal x-ray reflectivity profile [27]. A decrease in reflectivity around 0.8° is visible after implantation and remains after annealing. A Kiessig fringe located at 1° is visible after implantation. Both features show that the internal structure of the sample has changed [28]. The Kiessig fringe is the result of interference of reflected beams from internal surfaces with different refractive indices. After annealing, the Kiessig fringe disappears, indicating that the defects that gave rise to the change in refractive index have been healed by the thermal treatment.

The XRD measurements presented show an expansion of the *c* lattice parameter, providing evidence for the induced lattice damage. Although it is not possible to determine the type of defects associated with such damage, it becomes clear that some of these defects are annealed out by thermal treatments with the consequent lattice recovery, as concluded from the reflectivity measurements of figure 8. This annealing out of defects goes together with the reduction of the magnetic moment after annealing at 400 °C and with its disappearance after annealing at 500 °C, allowing association of these phenomena. The lower magnetic signal obtained for the highest implantation fluence can be explained by a high defect concentration, exceeding that needed for optimal magnetic band configuration, or alternatively by considering that the higher fluence promotes recombination and partial lattice reconstruction during implantation, as suggested by Esquinazi *et al* for the case of proton-irradiated graphite [26]. This latter argument is supported by the high radiation hardness attributed to ZnO, which requires more energy for defect production than other common semiconductor materials. Furthermore, RBS-channelling results show that lattice damage induced by implantation increases with fluence and saturates at about 5×10^{16} Ar cm^{-2}, with the formation of stable defect clusters but without amorphization of the structure [29]. Other experiments have shown the annealing of defects in ion-implanted ZnO to occur at temperatures as low as 300 °C [29, 30], which is in good agreement with the disappearance of the magnetic moment observed in the present work. One should recall that the ZnO single crystals come from the same batch and show no significant differences in impurity concentration.

Therefore, any difference in the magnetic signal must be related to the different implantation conditions.

4. Conclusions

Recent discussion on diluted magnetic semiconductors has focused on the role of lattice defects as at least partly responsible for the observed magnetic signal. In this work we give experimental evidence that lattice defects in bulk ZnO created by implantation with non-magnetic ions do give rise to a ferromagnetic signal. The high quality virgin crystals show traces of transition metal impurities but their magnetic moments are inert. The samples become ferromagnetic upon doping with Ar ions, the magnetic ordering extending above room temperature. The fact that ferromagnetic behaviour disappears after annealing at 500 °C can be explained by the annealing of the implantation defects, confirming the importance of lattice defects in the tailoring of the magnetic behaviour for this type of materials. There is mounting evidence on the role of defects in the magnetism of ZnO, while similar results may be observed for other oxide systems. Addressing questions such as defect characterization or determining their optimum concentration are some of the challenges lying ahead in the search for magnetic semiconductors.

Acknowledgments

The authors wish to acknowledge Jorge Rocha for the implantations and L C Alves for the PIXE analysis. R P Borges acknowledges FCT for support through grant SFRH/BPD/28221/2006.

References

[1] Dietl T, Ohno H, Matsukura F, Cibert J and Ferrand D 2000 *Science* **287** 1019
[2] Janisch R, Gopal P and Spaldin N A 2005 *J. Phys.: Condens. Matter* **17** R657
[3] Borges R P, Pinto J V, da Silva R C, Gonçalves A P, Cruz M M and Godinho M 2007 *J. Magn. Magn. Mater.* **316** e191
[4] Coey J M D, Venkatesan M, Stamenov P, Fitzgerald C B and Dorneles L S 2005 *Phys. Rev.* B **72** 024450
[5] Young D P, Hall D, Torelli M E, Fisk Z, Sarrao J L, Thompson J D, Ott H R, Oseroff S B, Goodrich R G and Zysler R 1999 *Nature* **397** 412
[6] Elfimov I S, Yunoki S and Sawatzky G 2002 *Phys. Rev. Lett.* **89** 216403
[7] Chaitania Das P and Sanvito S 2005 *Phys. Rev. Lett.* **94** 217205
[8] Coey J M D 2005 *Solid State Sci.* **7** 660
[9] Coey J M D 2006 *Curr. Opin. Solid State Mater. Sci.* **10** 83
[10] Schwartz D A and Gamelin D R 2004 *Adv. Mater.* **16** 2115
[11] Radovanovic P V and Gamelin D R 2003 *Phys. Rev. Lett.* **91** 157202
[12] Hong N H, Sakai J and Brizé V 2007 *J. Phys.: Condens. Matter* **19** 036219
[13] Sundaresan A, Bhargavi R, Rangarajan N, Siddesh U and Rao C N R 2006 *Phys. Rev.* B **74** 161306(R)
[14] Garcia M A *et al* 2007 *Nano Lett.* **7** 1489
[15] Dubroca T, Hack J, Hummel R E and Hangerhofer A 2006 *Appl. Phys. Lett.* **88** 182504
[16] Maxwell J A, Campbell J L and Teesdale W J 1989 *Nucl. Instrum. Methods* B **43** 218
Maxwell J A, Teesdale W J and Campbell J L 1995 *Nucl. Instrum. Methods* B **95** 407
[17] *CRC Handbook of Chemistry and Physics* 1999 80th edn (Boca Raton, FL: CRC Press) p 4-134
[18] Shim J H, Hwang T, Lee S, Park J H, Han S-J and Jeong Y H 2005 *Appl. Phys. Lett.* **86** 082503
[19] Chiou J W *et al* 2007 *Appl. Phys. Lett.* **90** 062103
[20] Kolesnik S, Dabrowski B and Mais J 2004 *J. Appl. Phys.* **95** 2582
[21] Blasco J, Bartolomé F, Garcia L M and Garcia J 2006 *J. Mater. Chem.* **16** 2282
[22] Wi S C *et al* 2004 *Appl. Phys. Lett.* **84** 4233
[23] Yin S *et al* 2006 *Phys. Rev.* B **73** 224408
[24] Potzger K *et al* 2006 *Appl. Phys. Lett.* **88** 052508

[25] Zhou S, Potzger K, Zhang G, Eichhorn F, Skorupa W, Helm M and Fassbender J 2006 *J. Appl. Phys.* **100** 114304
[26] Esquinazi P, Spemann D, Höhne R, Setzer A, Han K-H and Butz T 2003 *Phys. Rev. Lett.* **91** 227201
[27] Parratt L G 1954 *Phys. Rev.* **95** 2
[28] Born M and Wolf E 1980 *Principles of Optics* 6th edn (London: Pergamon)
[29] Lorenz K, Alves E, Wendler E, Bilani O, Wesch W and Hayes M 2005 *Appl. Phys. Lett.* **87** 191904
[30] Monteiro T, Boemare C, Soares M J, Rita E and Alves E 2003 *J. Appl. Phys.* **93** 8995